MATHEMATICAL MODELING AND COMPUTING, Vol. 12, No. 4, pp. 1243–1253 (2025)

Solving inverse problem of the potential theory by the cascade algorithm and the near-boundary element method

Zhuravchak L. M.[1], Zabrodska N. V.[2]

[1] *Lviv Polytechnic National University, 12 S. Bandera str., 79013, Lviv, Ukraine*
[2] *Carpathian Branch of S. I. Subbotin Institute of Geophysics of the National Academy of Sciences of Ukraine, 3b Naukova str., 79060, Lviv, Ukraine*

(Received 25 February 2025; Revised 13 November 2025; Accepted 30 November 2025)

The effectiveness of the indirect method of near-boundary elements (as a variant of the method of boundary integral equations) for constructing numerical solutions of direct and inverse problems of potential theory in a limited piecewise homogeneous object of arbitrary shape whose components are in ideal contact is substantiated. The integral representation of the solution of the direct problem is constructed using the fundamental solution of the Laplace equation for the plane. To find the intensities of unknown sources introduced in the near-boundary elements, the collocation technique was used, i.e. the boundary conditions of the first and second kinds and the conditions of ideal contact are satisfied in the middle of each boundary element. After solving the resulting system of linear algebraic equations, the unknown potential in the medium and inclusions and the flow through their boundaries are found, taking into account that the components are considered as completely independent domains. Based on the nature of the potential change or its derivative, the initial approximations for the conductivity of the inclusions, their centers of mass, orientation, and size are determined. To solve the inverse problem, an algorithm for recognizing the main physical and geometric characteristics of inclusions based on excess data of the potential or flow at the boundary of the object was built. It consists of two cascades of iterations: in the first of them, the location of inhomogeneities and their approximate sizes is determined, in the second one, it is specified their shape and orientation on the plane. A computational experiment was conducted for the problem of electrical exploration using a constant artificial field and the resistance method, in particular, electroprofiling.

Keywords: *mathematical modeling; potential theory; inverse problem; near-boundary element method; piecewise-homogeneous object; electrical profiling.*

2010 MSC: 60G35, 94A12 **DOI:** 10.23939/mmc2025.04.1243

1. Introduction

A mathematical model created according to the original physical parameters for obtaining information about the object's behavior, in contrast to a real experiment, has a number of advantages related to such basic aspects. It saves the material resources necessary for conducting a physical experiment, makes it possible to test the system in extreme conditions and even beyond their limits (for example, to investigate the process of heating to hundreds of degrees at rates lower than tenths of a degree per hour), as well as to evaluate its performance with long-term technological work cycles (days, weeks, months, years) in significantly shorter terms. From a mathematical point of view, the model is mostly a system of differential equations in partial derivatives, which describes the behavior of the object in the environment with established boundary and initial (for a non-stationary process) conditions. Solutions of direct problems of potential theory can be the following physical quantities: temperature and heat flow (when simulating a thermal field), potential difference and current density (when simulating an electric field), diffusion and diffusion flow (when simulating a diffusion field),

displacements, deformations and surface forces (when modeling the stress-strain state). Analytical and numerical methods of solution have been developed in detail for direct problems of potential theory, the most popular of which are the methods of finite differences, finite, boundary and near-boundary elements. To implement the listed methods, packages of application programs have been created, which are constantly being improved [1–11].

Using a mathematical model, researchers establish connections between input and output data about the object and predict its behavior in response to changes in external factors. Together with the additional experimental data provided by the problem setter, it is the result of the first stage of simulation. Since, during the description of real processes, the values of some physical characteristics and geometric parameters included in the model equations are taken with significant assumptions, they can be considered as unknown values for the specific task of mathematical modeling. For their determination, additional indirect information about the research object should be used: experimentally obtained data on the solution of the problem. This is how inverse problems are formulated, which, unlike direct problems, from a mathematical point of view belong to the class of incorrect problems, since their solution is unstable with respect to input data errors [12–14]. The elimination of problems related to the incorrectness of the task is carried out at the second stage of modeling by developing special regulatory algorithms [15, 16].

For the inverse problems of potential theory, it is necessary to determine one or more factors based on known (observable) functions: external influence; boundary conditions formulated for the model; coefficients of differential operators applied to its model and related to the structure of the object, its physical and chemical properties; its geometric parameters. By solving inverse problems, researchers determine the mechanical and thermophysical properties of materials, identify polymer and composite materials, biomaterials, piezoceramic materials; solve electrical prospecting tasks, in particular, determine the location and capacity of mineral deposits; solve the problems of non-destructive testing, in particular, determine the location and configuration of the defect by the field of elastic movements measured on the body surface or by resonance frequencies; simulate the phenomena of acoustic emission and establish a connection between the main characteristics of the emission and the stress state, the study of this phenomenon allows to reveal the state of the structure, which precedes its destruction; solve the problems of X-ray and acoustic tomography.

2. Problem formulation

Let it be necessary to determine the geometric parameters of the inclusions according to the nature of the scalar potential and (or) the flow of the potential field at the boundary $\partial\Omega$ of the piecewise-homogeneous object, which occupies the domain Ω in the Cartesian coordinate system (x_1, x_2). We assume that within the domain Ω_0 the potential $u_0(x)$ of the stationary physical field, which is used to recognize the internal physical and geometric structure of the object, satisfies the equation

$$P(u_0(x)) = \Delta u_0(x) = \sigma_0 \left(\frac{\partial^2 u_0(x)}{\partial x_1^2} + \frac{\partial^2 u_0(x)}{\partial x_2^2} \right) = -g_0(x)\chi_g(x), \quad x \in \Omega_0, \tag{1}$$

everywhere, with the exception of an unknown number M of inclusions Ω_m ($\cup_{m=1}^{M} \Omega_m \subset \Omega$), here $\chi_g(x)$ is the characteristic function of the domain Ω_g ($\Omega_g \subset \Omega_0$), in which the sources are located, $x = (x_1, x_2)$.

In the domains Ω_m the environments are homogeneous, but different from the one in which the operator $P(u_0(x))$ operates, so the process in them is described by equations

$$P(u_m(x)) = \Delta u_m(x) = \sigma_m \left(\frac{\partial^2 u_m(x)}{\partial x_1^2} + \frac{\partial^2 u_m(x)}{\partial x_2^2} \right) = 0, \quad x \in \Omega_m. \tag{2}$$

Here σ_s ($s = \overline{0, M}$) is a constant physical characteristic (coefficient of thermal conductivity, electrical conductivity, magnetic permeability, etc.).

Boundary conditions of the first and second kind are specified on the boundary sections $\partial\Omega^{(i)} \subset \partial\Omega$ ($i = 1, 2$):

$$u_0(x) = u_\Gamma(x), \quad x \in \partial\Omega^{(1)}, \qquad q_0(x) = -\sigma_0 \frac{\partial u_0(x)}{\partial \mathbf{n}(x)} = q_\Gamma(x), \quad x \in \partial\Omega^{(2)}, \tag{3}$$

where $x = (x_1, x_2)$, $\partial\Omega = \partial\Omega^{(1)} \cup \partial\Omega^{(2)}$, $\mathbf{n}(x) = (n_1(x), n_2(x))$ is a uniquely defined external unit normal to the boundary $\partial\Omega_0 = \partial\Omega \cup (\cup_{m=1}^{M} \partial\Omega_m)$.

In addition, for the mathematical formulation of the excess of boundary conditions necessary for solving the inverse problem, we consider that boundary conditions of the second and first kind, respectively, are also specified on the sections $\partial\Omega_b^{(i)} \subset \partial\Omega^{(i)}$:

$$q_0(x) = q_b(x), \quad x \in \partial\Omega_b^{(1)}, \qquad u_0(x) = u_b(x), \quad x \in \partial\Omega_b^{(2)}. \tag{4}$$

Note that for the correct statement of direct problems of mathematical physics $\partial\Omega_b = \partial\Omega_b^{(1)} \cup \partial\Omega_b^{(2)}$ must be an empty set. When solving inverse problems, its presence is mandatory, and the quality and reliability of the result is higher, the smaller the area of $\partial\Omega^{(i)} \backslash \partial\Omega_b^{(i)}$ is, that is, it is best when the ratio $\partial\Omega^{(i)} \backslash \partial\Omega_b^{(i)} = \varnothing$ is fulfilled.

The ideal contact conditions are set at the interface boundaries $\partial\Omega_m$:

$$u_0(x) = u_m(x), \quad -\sigma_0 \frac{\partial u_0(x)}{\partial \mathbf{n}(x)} = -\sigma_m \frac{\partial u_m(x)}{\partial \mathbf{n}(x)}, \quad x \in \partial\Omega_m, \quad m = \overline{1, M}. \tag{5}$$

Let us model $\partial\Omega_m$ by N linear segments $\tilde{\Gamma}_n^m$ $(n = 1, \ldots, N)$, which we set as follows: $(x_{1n}^m, x_{2n}^m) \in \tilde{\Gamma}_n^m$, if $x_{1n}^m = x_{1n}^{m1}\varphi_1(\eta) + x_{1n}^{m2}\varphi_2(\eta)$, $x_{2n}^m = x_{2n}^{m1}\varphi_1(\eta) + x_{2n}^{m2}\varphi_2(\eta)$, where $\left(x_{1n}^{m1}, x_{2n}^{m1}\right)$ and $\left(x_{1n}^{m2}, x_{2n}^{m2}\right)$ are the coordinates of the extreme points of the segment $\tilde{\Gamma}_n^m$, $\varphi_1(\eta) = 0.5(\eta - 1)\eta$, $\varphi_2(\eta) = 0.5(\eta + 1)\eta$, η is a one-dimensional coordinate that changes from -1 to 1 when the point (x_{1n}^m, x_{2n}^m) moves from $\left(x_{1n}^{m1}, x_{2n}^{m1}\right)$ to $\left(x_{1n}^{m2}, x_{2n}^{m2}\right)$ along the segment $\tilde{\Gamma}_n^m$. Since the closed fracture simulating $\partial\Omega_m$ is continuous, we will require that $\left(x_{1n}^{m2} = x_{1(n+1)}^{m1}\right)$, $\left(x_{2n}^{m2} = x_{2(n+1)}^{m1}\right)$ for $n < N$ and $\left(x_{1n}^{m2} = x_{11}^{m1}\right)$, $\left(x_{2n}^{m2} = x_{21}^{m1}\right)$ for $n = N$.

We note that at the initial stages it is advisable to limit ourselves to the case of $N = 4$. Finding unknown values x_{1n}^{m1}, x_{2n}^{m1}, x_{1n}^{m2}, x_{2n}^{m2} will be carried out in stages. First, we write down the algorithm for solving the direct problem of potential theory, then we consider them known, and then we build a method for recognizing the physical and geometric parameters of inclusions Ω_m.

3. Algorithm for solving the direct potential theory problem

We will find solutions to the problem (1)–(3), (5), using the indirect near-boundary element method (NBEM) [17, 18]. To construct the solution, we will use the fundamental solutions of Laplace's equations:

$$\mathbf{E}_s(x, \xi) = \mathbf{E}_s(r) = -\frac{1}{2\pi\sigma_s} \ln |r/r_0|, \quad s = \overline{0, M}, \tag{6}$$

and their derivatives along the normal:

$$\mathbf{F}_s(x, \xi) = \mathbf{F}_s(r) = \sigma_s \sum_{i=1}^{2} \frac{n_i(x)\,(x_i - \xi_i)}{2\pi r^2}.$$

Here ξ_1, ξ_2 is the coordinate system that coincides with x_1, x_2, the constant r_0 is used to improve the accuracy of the calculations, $r^2 = (x_1 - \xi_1)^2 + (x_2 - \xi_2)^2$.

Step 1. We divide the boundaries $\partial\Omega_m$ into boundary elements Γ_{mv} so that $\cup_{v=1}^{V_m} \Gamma_{mv} = \partial\Omega_m$, $\Gamma_{mv} \cap \Gamma_{mq} = \varnothing$, $v \neq q$, $v, q = \overline{1, V_m}$. We introduce external boundary regions $G_s = B_s/\Omega_s$, where $B_s \subset \mathbf{R}_s^2$, $\Omega_s \subset B_s$, $\partial B_s \cap \partial\Omega_s = \varnothing$, and each G_s divide into elements G_{sv} so that each boundary element Γ_{mv} corresponds to two near-boundary ones G_{mv} and G_{0v}: $G_{mv} \cap \partial\Omega_m = \Gamma_{mv}$, $G_{0v} \cap \partial\Omega_m = \Gamma_{mv}$, $G_{sv} \cap G_{sq} = \varnothing$, $v \neq q$, $v, q = \overline{1, V_s}$, $\cup_{v=1}^{V_s} G_{sv} = G_s$, $V_0 = \sum_{m=1}^{M} V_m$. On each of the boundary elements G_{sv} we introduce fictitious sources of unknown intensity $g_{sv}(\xi)$.

Step 2. We approximate the intensities of unknown sources $g_{sv}(\xi)$ by constants d_{sv} and we pass from differential equations (1), (2) to their integral representations, that is, we write the potentials and their derivatives along the normal in the form:

$$u_0(x) = \sum_{v=1}^{V_0} d_{0v} \int_{G_{0v}} \mathbf{E}_0(x,\xi)\, dG_{0v}(\xi) + \int_{\Omega_g} \mathbf{E}_0(x,\xi)\, g_0(\xi)\, d\Omega_g(\xi) + C_0,$$

$$u_m(x) = \sum_{v=1}^{V_m} d_{mv} \int_{G_{mv}} \mathbf{E}_m(x,\xi)\, dG_{mv}(\xi) + C_m, \tag{7}$$

$$q_0(x) = \sum_{v=1}^{V_0} d_{0v} \int_{G_{0v}} \mathbf{F}_0(x,\xi)\, dG_{0v}(\xi) + \int_{\Omega_g} \mathbf{F}_0(x,\xi)\, g_0(\xi)\, d\Omega_g(\xi),$$

$$q_m(x) = -\sigma_m \frac{\partial u_m(x)}{\partial \mathbf{n}} = \sum_{v=1}^{V_m} d_{mv} \int_{G_{mv}} \mathbf{F}_m(x,\xi)\, dG_{mv}(\xi). \tag{8}$$

Note that, except for the inclusion boundaries, (7) satisfies (1), (2) exactly in Ω. This fact frees us from constructing a mesh in Ω.

Step 3. To find the intensities of unknown sources, we will use the collocation method, i.e., the conditions of ideal contact will be satisfied in the middle of each boundary element. Substituting (7), (8) into (3), (5) and adding the condition of equality of zero in $\mathbf{R}_s^2$ of the sum of all sources at infinity, we will obtain a system of linear algebraic equations (SLAE) for finding the unknowns d_{sv} and C_s:

$$\sum_{v=1}^{V_0} d_{0v} \int_{G_{0v}} \mathbf{E}_0(x^w,\xi)\, dG_{0v}(\xi) + \int_{\Omega_g} \mathbf{E}_0(x^w,\xi)\, g_0(\xi)\, d\Omega_g(\xi) + C_0 = u_\Gamma(x^w), \quad x^w \in \partial\Omega^{(1)},$$

$$\sum_{v=1}^{V_0} d_{0v} \int_{G_{0v}} \mathbf{F}_0(x^w,\xi)\, dG_{0v}(\xi) + \int_{\Omega_g} \mathbf{F}_0(x^w,\xi)\, g_0(\xi)\, d\Omega_g(\xi) = q_\Gamma(x^w), \quad x^w \in \partial\Omega^{(2)}, \tag{9}$$

$$\sum_{v=1}^{V_0} d_{0v} \int_{G_{0v}} \mathbf{E}_0(x^w,\xi)\, dG_{0v}(\xi) - \sum_{v=1}^{V_m} d_{mv} \int_{G_{mv}} \mathbf{E}_m(x^w,\xi)\, dG_{mv}(\xi) + C_0 - C_m$$
$$- \int_{\Omega_g} \mathbf{E}_0(x^w,\xi)\, g_0(\xi)\, d\Omega_g(\xi), \quad x^w \in \partial\Omega_m, \quad m = \overline{1,M}, \tag{10}$$

$$\sum_{v=1}^{V_0} d_{0v} \int_{G_{0v}} \mathbf{F}_0(x^w,\xi)\, dG_{0v}(\xi) - \sum_{v=1}^{V_m} d_{mv} \int_{G_{mv}} \mathbf{F}_m(x^w,\xi)\, dG_{mv}(\xi) = - \int_{\Omega_g} \mathbf{F}_0(x^w,\xi)\, g_0(\xi)\, d\Omega_g(\xi),$$
$$x^w \in \partial\Omega_m, \quad m = \overline{1,M}, \tag{11}$$

$$\sum_{v=1}^{V_s} d_{sv} \int_{G_{sv}} dG_{sv}(\xi) + C_s = 0, \quad s = \overline{0,M}.$$

Step 4. After finding the unknown values d_{sv} and C_s as solutions of the SLAE (9)–(11), the unknown potential in the medium and inclusions and the flow through their boundaries are calculated using the formulas (7), (8), since the medium and inclusions are now considered as completely independent regions.

4. Solving the inverse problem of potential theory

We store the geometric information about each $\partial\Omega_m$ in the form of N pairs of numbers (x_{1n}^m, x_{2n}^m). Now, if we take into account that they are included in the integral representations (7), (8) by rather complex expressions, and also that we will use iterative procedures to find them, then it is advisable to reduce the number of unknowns at the first stages of recognition. To do this, we will introduce additional dependencies between the vertices x_{1n}^m, x_{2n}^m and the centers of mass of the inclusions (x_{10}^m, x_{20}^m) and limit ourselves to the case $N = 4$ for each inclusion.

We organize the iterative recognition algorithm as follows [19].

Step 1. Taking into account the acquired experience and the previous qualitative analysis of the behavior of $u_0(x)$ on $\partial\Omega_b^{(2)}$ or $q_0(x)$ on $\partial\Omega_b^{(1)}$, we set the initial (zero) approximations for all parameters: M_0, $\Delta\sigma_m$, (x_{10}^m, x_{20}^m) is the center of mass of each inclusion, modeled by a rectangle with sides $2l_1^m$, $2l_2^m$ or a rhombus with equal diagonals of length $2l_0^m$.

Step 2. We set $\sigma_m = \sigma_0 + \Delta\sigma_m$, assuming that σ_0 is known.

Step 3. We organize the first cascade of iterations to specify the location of inhomogeneities and their approximate sizes.

1. We model $\partial\Omega_m$ as a rectangle or rhombus with vertex coordinates:

$$\begin{gathered} x_{11}^m = x_{10}^m - l_1^m, \quad x_{21}^m = x_{20}^m - l_2^m, \quad x_{12}^m = x_{10}^m + l_1^m, \quad x_{22}^m = x_{20}^m - l_2^m, \\ x_{13}^m = x_{10}^m + l_1^m, \quad x_{23}^m = x_{20}^m + l_2^m, \quad x_{14}^m = x_{10}^m - l_1^m, \quad x_{24}^m = x_{20}^m + l_2^m, \\ x_{11}^m = x_{10}^m - l_0^m, \quad x_{21}^m = x_{20}^m, \quad x_{12}^m = x_{10}^m, \quad x_{22}^m = x_{20}^m - l_0^m, \\ x_{13}^m = x_{10}^m + l_0^m, \quad x_{23}^m = x_{20}^m, \quad x_{14}^m = x_{10}^m, \quad x_{24}^m = x_{20}^m + l_0^m. \end{gathered} \tag{12}$$

2. For the selected σ_m, using the above-described algorithm for solving the direct problem, we calculate the potential $u_0(x)$ by the formula (7) for $x \in \partial\Omega_b^{(2)}$ or the normal derivative of the potential $q_0(x)$ by the formula (8) for $x \in \partial\Omega_b^{(1)}$.

3. Taking into account the conditions (4), we minimize the functional

$$I_1^0 = \int_{\partial\Omega_b^{(2)}} |u_b(x) - u_0(x)|\, d\partial\Omega_b^{(2)}(x)$$

or

$$I_2^0 = \int_{\partial\Omega_b^{(1)}} |q_b(x) - q_0(x)|\, d\partial\Omega_b^{(1)}(x), \tag{13}$$

allowing variation only x_{10}^m, x_{20}^m, l_0^m (or l_1^m, l_2^m).

4. Fixing x_{10}^{mf}, x_{20}^{mf}, l_0^{mf} (or l_1^{mf}, l_2^{mf}), which correspond to the found minimum of the functional (13) and refine the electrical conductivity σ_m by minimization (13), we will denote them as σ_m^f.

5. As a result, we will find, using a formula similar to (12), the refined coordinates of the vertices of a rectangle or rhombus $(x_{1n}^{mf}, x_{2n}^{mf})$, $n = 1, \ldots, 4$.

Step 4. We organize a second cascade of iterations to refine the shape and orientation in the inclusion space.

1. We will rotate the rectangle or rhombus found in step 3 around its center of mass, while scaling along the axes. To do this, we introduce three new parameters for each inclusion: φ_0^m, s_1^m, s_2^m and calculate the new coordinates of the vertices of the rectangle or rhombus:

$$\begin{gathered} x_{1n}^{mr} = \left(x_{1n}^{mf} - x_{10}^{mf}\right)\cos\varphi_0^m - \left(x_{2n}^{mf} - x_{20}^{mf}\right)\sin\varphi_0^m + x_{10}^{mf}, \\ x_{2n}^{mr} = \left(x_{1n}^{mf} - x_{10}^{mf}\right)\sin\varphi_0^m + \left(x_{2n}^{mf} - x_{20}^{mf}\right)\cos\varphi_0^m + x_{20}^{mf}, \\ x_{1n}^{mc} = x_{1n}^{mr} s_1^m + \left(1 - s_1^m\right)x_{10}^{mf}, \quad x_{2n}^{mc} = x_{2n}^{mr} s_2^m + \left(1 - s_2^m\right)x_{20}^{mf}. \end{gathered} \tag{14}$$

2. We minimize the functional (13) by varying φ_0^m, s_1^m, s_2^m and fix φ_0^{mf}, s_1^{mf}, s_2^{mf}, which correspond to the found minimum.

3. For constants x_{10}^{mf}, x_{20}^{mf}, l_0^{mf} (or l_1^{mf}, l_2^{mf}), φ_0^{mf}, s_1^{mf}, s_2^{mf} we refine the electrical conductivity σ_m^f by minimizing (13), we denote it by σ_m^{f2}.

Step 5. The found values x_{1n}^{mc}, x_{2n}^{mc} serve instead of the variables x_{1n}^{mf}, x_{2n}^{mf} in the formulas (14) for further refinement in the iterative process of minimization (13) with constants σ_m^{f2}. Note that the last two steps are sometimes advisable to repeat several times.

It is obvious that the geometric coordinates and physical characteristics of the inclusions are real numbers and have the possibility of continuous change, so standard gradient-minimization procedures could be applied to them. However, due to the existence of the integer parameter M, the use of the above methods is somewhat complicated.

Step 6. Along with the initial approximation, estimated as having the highest probability, we take into account two "neighboring" approximations with parameters $M_+ = M_0 + 1$ and $M_- = M_0 - 1$. These three initial approximations form a model, which we will call three-leaves one. It is clear that M_0 is not equal to zero, and in the case $M_0 = 1$ on the leaf corresponding to $M_0 - 1$ we check the situation when there is no inclusion in the homogeneous body. In the process of minimizing the functionals I_1^0 or I_2^0, I_1^+ or I_2^+, I_1^- or I_2^-, calculated by formulas (13), two qualitative restructurings of the model are provided:

1) transition to another triple of leaves in the case when $I^0 + \delta > I^+$ or $I^0 - \delta < I^-$, where δ is the number that characterizes the transition threshold;

2) refinement of the approximation of the boundary $\partial\Omega_m$, i.e. introduction of an additional number of boundary elements; it is carried out when a local minimum is reached for some parameters.

5. Testing the developed approach

The direct and inverse problems of direct current electrical exploration using electrical profiling were solved. The Earth's crust was modeled by a piecewise homogeneous isotropic half-plane $R^{2-} = \{(x_1, x_2) : -\infty < x_1 < \infty, -\infty < x_2 < 0\}$ with an electrically insulated boundary $\Gamma = \{(x_1, x_2) : -\infty < x_1 < \infty, x_2 = 0\}$ in the Cartesian coordinate system x_1, x_2. That means the condition $q_2(x) = 0$ was fulfilled everywhere on the boundary except for the points $A = (-25, 0)$ and $B = (25, 0)$, in which current sources were placed – feed electrodes with intensity $g_A = -0.5$ and $g_B = 0.5$, respectively. The current strength I and the electrical conductivity σ_0 of the geological environment Ω_0 were set equal to unity. The distance between the receiving electrodes was chosen $N = 0.1$ and they were moved along the line $(-25, 25)$ with a step of 0.1.

To construct the solution to problem (1)–(3), (5), fundamental solutions (6) for inclusions and a special fundamental solution for the half-space (Green's function) of the Laplace equation (1) were used:

$$\mathbf{E}_{0h}(r) = \mathbf{E}_0(r) + \mathbf{E}_0(r'),$$

where $r'^2 = (x_1 - \xi_1)^2 + (x_2 + \xi_2)^2$.

It automatically satisfies the zero boundary condition of the second kind from (3).

The SLAE for finding the unknowns d_{sv} and $_m$ consists of equations (10) (in which the constant C_0 is absent), (11) and M equations for inclusions below (11), where $g_0(\xi) = 2(g_A + g_B)/\sigma_0$.

The dependence of the apparent resistivity (the inverse value of electrical conductivity)

$$\rho = (k_u/I)|u_0(x_M) - u_0(x_N)|$$

on the number of inclusions, their shape, depth of occurrence and size is investigated. Here $k_u = 2\pi(1/\ln r_{AM} - 1/\ln r_{AN} - 1/\ln r_{BM} + 1/\ln r_{BN})^{-1}$ is the coefficient of installation ABMN. It is clear that the apparent resistivity of a homogeneous half-plane is equal to unity at each point.

In order to obtain recommendations for finding initial approximations of the characteristics, we first solve a series of direct problems of the potential theory for two rectangular inclusions with sides $2l_m^1$, $2l_2^m$ $(m = 1, 2)$, located at depths h_1, h_2 horizontally at a distance s from each other, i.e. their longer sides are parallel to the day surface.

Figures 1–3 illustrate the apparent resistivity (the inverse value of the electrical conductivity) registered on the day surface, with some variable parameters of the mathematical model and the same depth of both inclusions ($h_1 = h_2 = 2$) and a constant distance between them ($s = 4$). Since it is more difficult to establish regularities when the geometric and physical characteristics of both inclusions change simultaneously, we do not change the characteristics of the first inclusion ($l_1^1 = 2$, $l_2^1 = 1$, $\rho_1 = 2$) but change in the second one. It is clear that with variable characteristics of the first inclusion and constant characteristics of the second one, the apparent resistivity graphs will be a mirror image of those shown.

Figure 1 shows graphs of the apparent resistivity dependence upon changes in the resistance of the second inclusion for the same inclusion sizes ($l_1^2 = 2$, $l_2^2 = 1$). The convexity (concavity) of the graph

indicates that the resistivity of the inclusion is greater (less) than the resistivity of the medium, so we assume $\Delta\sigma$ can be negative (positive). An increase in the resistance of the inclusion is manifested by larger maximum on the curves, and its decrease by smaller minimum in the area above the second inclusion.

Figure 2 shows graphs of the apparent resistivity upon changes in the vertical size (height) of the second inclusion for the same resistances of the inclusions ($\rho_2 = 2$). Here we observe an increase in the maximum with increasing height. Although the electrical profiling method is usually used to study the structure along the lateral, these graphs show a directly proportional relationship between the vertical size of the inclusion and the maximum value of the apparent resistivity calculated on the dayside surface.

Figure 3 shows graphs of the apparent resistivity when changing the horizontal size (length) of the second inclusion for the same resistances of the inclusions ($\rho_2 = 2$). We see that with increasing length, the distance between the minima of the section of the curve above the second inclusion increases in direct proportion.

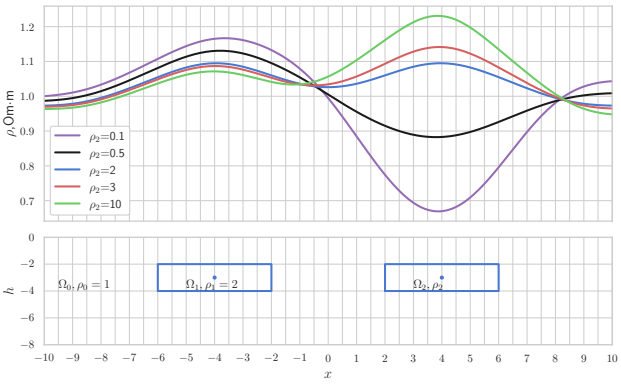

Fig. 1. Graphs of the apparent resistivity dependence upon changes in the resistance of the second inclusion.

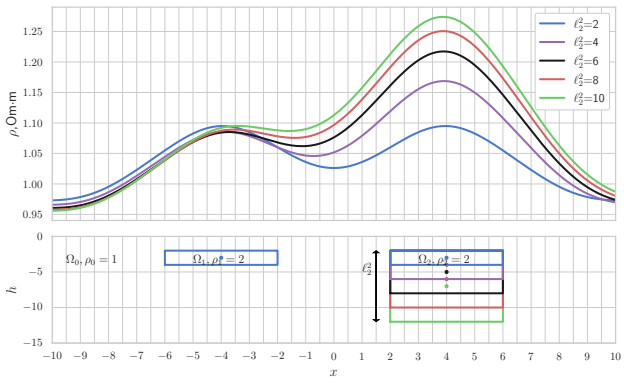

Fig. 2. Graphs of the apparent resistivity upon changes in height of the second inclusion.

Figures 4–6 illustrate the apparent resistivity recorded on the day surface, with some variable parameters of the mathematical model and the same sizes ($l_1^2 = 2$, $l_2^2 = 1$) and resistances ($\rho_2 = 2$) of both inclusions.

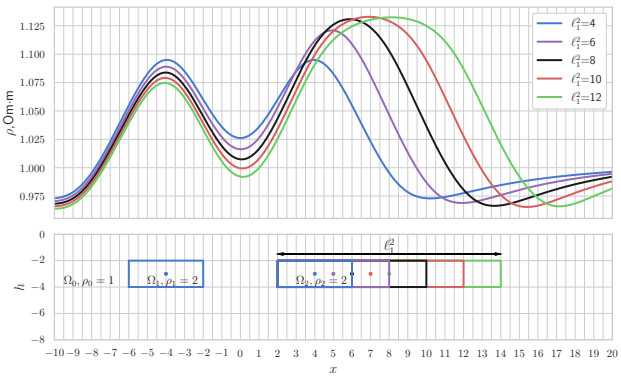

Fig. 3. Graphs of the apparent resistivity upon changes in length of the second inclusion.

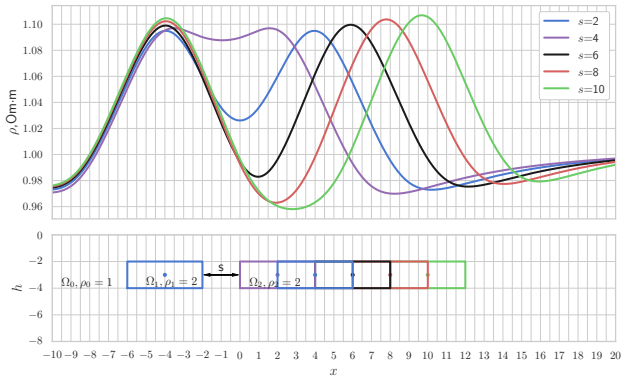

Fig. 4. Graphs of the apparent resistivity upon changes in the distance between the inclusions.

Figure 4 shows the graphs of the apparent resistivity when the distance s between the inclusions changes with their same sizes and resistances. It is easy to see that the increase of the distance between the inclusions is also directly proportional to the increase of the distance between the maxima on the observed curves.

Figure 5 shows the graphs of the apparent resistivity when the distance h_2 of the second inclusion changes from the dayside surface (the boundary of the medium). It is seen that with increasing depth, the value of the maximum corresponding to the second inclusion decreases, and the inclusion will no longer be identified at a depth greater than $h_2 = 5$.

Figure 6 shows graphs of apparent resistivity when changing the orientation (angle of inclination) of the rectangular inclusion at a constant distance between them ($s = 4$) and a constant depth of the center of mass of the second inclusion ($h_2 + l_2^2 = 2 + 1$). The dependence is manifested by a change in the position of the maxima both horizontally and vertically.

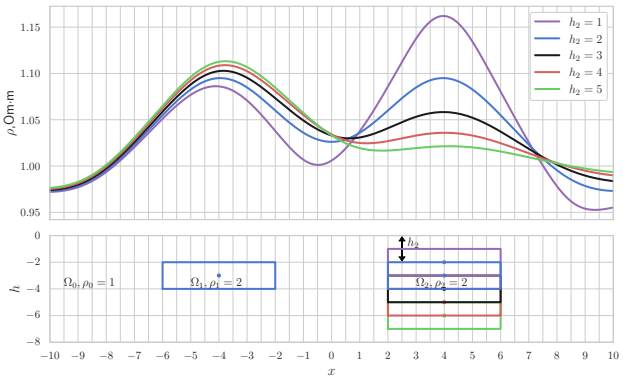

Fig. 5. Graphs of the apparent resistivity upon changes in the depth of the second inclusion.

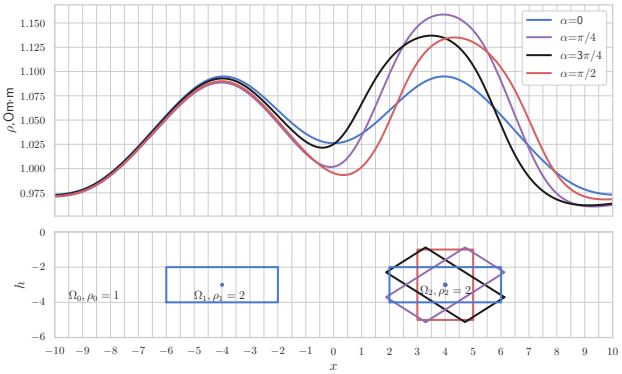

Fig. 6. Graphs of apparent resistivity upon changes in the orientation of the second inclusion.

As one can see, two inclusions in the half-plane can be identified by the presence of two extrema on the curve section, and the even (second and fourth) extrema correspond to the centers of mass of the inclusions, the third (if it is present) indicates the middle of the segment connecting the inclusions.

Having some information about the research area from previous experience, we determine the initial approximations and the possible range of parameters that we need to find.

Having found the initial approximations, we calculate the functional for fives fixed parameters (l_1^m, l_2^m, s) and two variable ones ($h = h_2$ and $\rho = \rho_1 = \rho_2$). From Figures 7, 8 we see (both in the three-dimensional image and on the isolines) that there is a section where the value of the functional is the smallest, and it indicates a possible solution to the problem: $h = \rho = 2$.

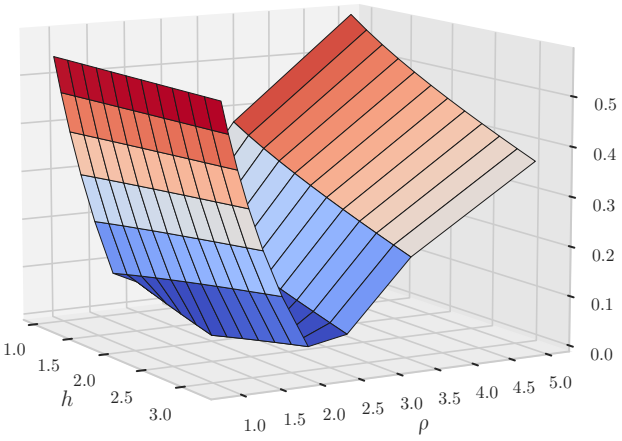

Fig. 7. 3D-graph of functional.

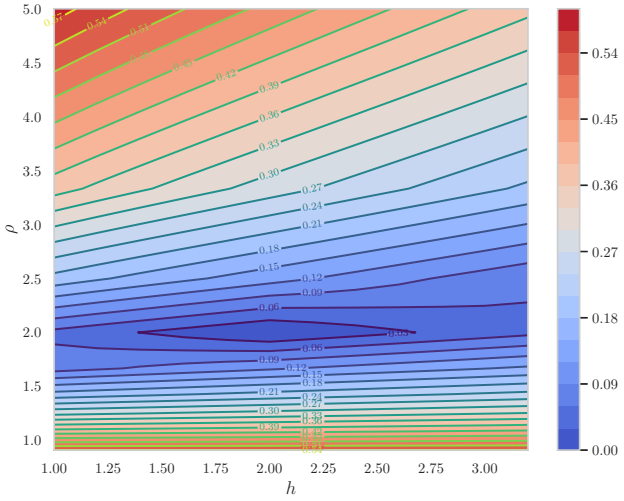

Fig. 8. Isoline plots of functional.

It is generally accepted that one solution of the inverse problem (in our case, one apparent resistivity curve) may correspond to several variants of the location of inclusions of different electrical conductivity in the medium. Despite the visual similarity of the apparent resistivity graphs obtained solving the

direct potential theory problem, the proposed cascade algorithm for solving the inverse problem allows us to state that for one such graph there is only one set of geometric and physical characteristics of inclusions and the medium that corresponds to it. Therefore, the use of NBEM, which is the high-precision numerical method, significantly increases the probability that only one set of characteristics of inclusions and the medium corresponds to one curve.

6. Conclusions

1. During the preliminary interpretation, a priori information about the geoelectric section was obtained: the number of inclusions, approximate values of their lengths and resistivities. Among the methods and algorithms for solving direct problems of electrical exploration, the indirect method of near-boundary elements was selected, which is characterized by high accuracy and acceptable calculation time, step-by-step stages of entering additional information. To obtain a priori parameters of the model, a number of direct problems were solved and theoretical curves were compared with the curve obtained in experimental studies. For the best coincidence of the experimental curve with the theoretical ones, the model parameters were gradually changed. The method of successive approximations was used to obtain the minimum deviation of apparent resistivities for all depth parameters.

2. The ambiguity of the solution of inverse electrical exploration problems leads to the existence of a set of equivalent solutions. For low-power inclusions, when their thickness is comparable to the thickness of the overlying layer or is smaller, errors in determining the thicknesses of inclusions and apparent resistances can reach tens and hundreds of percent regardless of the interpretation method. Therefore, the use of special algorithms for computer interpretation makes it possible to assess the limits of the equivalence principle, i.e. to find physical errors in determining not only the thicknesses of inclusions and apparent resistances, but also the longitudinal conductivities and transverse resistances of inclusions.

3. The most reliable parameters for various inclusions of the studied section are the main result of the formal physical and mathematical interpretation of electrical exploration data. They can be used to obtain geological and hydrogeological characteristics of rocks: fracturing, waterlogging, speed of movement or filtration of groundwater, degree of contamination, salinity of soils, groundwater, etc.

4. To obtain the remaining parameters (especially the height of inclusions), additional information is required about the electromagnetic properties of intermediate horizons (most often about specific resistances). Such information is obtained by conducting electromagnetic studies in wells, using seismic data, detailed analysis of all geological and geophysical information in the area, mutual correlation of data of group interpretation of electromagnetic sounding data in neighboring areas.

5. The shape and extension of electric field anomalies mainly correspond to the spatial arrangement of the objects that created them. The width of the anomaly over a thin object depends on the depth of its upper edge, and over a thick one – on its thickness. The shape and intensity of anomalies, and therefore the efficiency of profiling, depend on the following natural and technical factors: the depth of occurrence h in relation to the transverse dimensions d of geological objects (objects with h/d less than 2–5 are mainly distinguished); the contrast of the electromagnetic properties of objects and the containing environment; the level of technical interference and the presence of interference-protected equipment; the optimal choice of the method, the depth of exploration, the observation system, the intensity of the primary (feed) field and its polarization, i.e. the direction of the electric field vector relative to the extension of the objects.

6. In further research, we plan to expand the proposed algorithm for solving the inverse problem using the vertical electrical sensing method for two inclusions placed vertically, of the same and different electrical conductivity, and also to develop an algorithm for recognizing the characteristics of one inclusion for the case of induced polarization.

[1] Lv M., Zhang Y., Liu S. Fast forward approximation and multitask inversion of gravity anomaly based on UNet3+. Geophysical Journal International. **234** (2), 972–984 (2023).

[2] Milson J., Eriksen A. Field Geophysics. John Wiley & Sons, Ltd (2011).

[3] Van Baal P. A Course in Field Theory. CRC Press (2014).

[4] Qu W., Chen W., Fu Z. Solutions of 2D and 3D non-homogeneous potential problems by using a boundary element-collocation method. Engineering Analysis with Boundary Elements. **60**, 2–9 (2015).

[5] Zhdanov M. S. Geophysical Electromagnetic Theory and Methods. Elsevier Science. **43** (2009).

[6] Brebbia C. A., Telles J. C. F, Wrobel L. C. Boundary Element Techniques: Theory and Applications in Engineering. Springer Berlin, Heidelberg (2012).

[7] Foks N. L., Krahenbuhl R., Li Y. Adaptive sampling of potential-field data: A direct approach to compressive inversion. Geophysics. **79** (1), 17JF–Z24 (2014).

[8] Zhang Y., Qu W., Chen J. A new regularized BEM for 3D potential problems. Scientia Sinica Physica, Mechanica & Astronomica. **43** (3), 297–308 (2013).

[9] Zhuravchak L. M., Kruk O. S. Consideration of the nonlinear behavior of environmental material and a three-dimensional internal heat sources in mathematical modeling of heat conduction. Mathematical Modeling and Computing. **2** (1), 107–113 (2015).

[10] Zhuravchak L. M., Zabrods'ka N. V. Nonstationary thermal fields in inhomogeneous materials with nonlinear behavior of the components. Materials Science. **46** (1), 36–46 (2010).

[11] Havrysh V. I., Kolyasa L. I., Ukhanska O. M., Loik V. B. Determination of temperature field in thermally sensitive layered medium with inclusions. Naukovyi Visnyk Natsionalnoho Hirnychoho Universytetu. **1**, 76–82 (2019).

[12] Mikheeva T., Lapina O., Kyshman-Lavanova T., Prychepiy T. Geophysical data interpretation technologies in the study and exploration of oil-and-gas deposits. Geofizicheskiy Zhurnal. **44** (5), 106–122 (2023).

[13] Mukanova B., Modin I. The Boundary Element Method in Geophysical Survey. Springer Cham (2018).

[14] Bomba A. Y., Boichura M. V. Identifying the structure of soil massifs by Numerical Quasiconformal Mapping Methods. Cybernetics and System Analysis. **57** (6), 927–937 (2021).

[15] Zhou S., Jia H., Lin T., Zeng Z., Yu P., Jiao J. An accelerated algorithm for 3D inversion of gravity data based on improved conjugate gradient method. Applied Sciences. **13** (18), 10265 (2023).

[16] Li Z., Ma G., Meng Q., Wang T., Li L. Gravity and magnetic fast inversion method with cross-gradient based on function fitting. Geophysical Journal International. **2**, 1209–1218 (2022).

[17] Zhuravchak L. Computation of pressure change in piecewise-homogeneous reservoir for elastic regime by indirect near-boundary element method. 2019 IEEE 14th International Conference on Computer Sciences and Information Technologies (CSIT). 141–144 (2019).

[18] Zhuravchak L. M. Potential field modeling by combination of near-boundary and contact elements with non-classical finite differences in a heterogeneous medium. Mathematical Modeling and Computing. **11** (2), 373–384 (2024).

[19] Zhuravchak L., Zabrodska N. Algorithm for determining inclusion parameters in solving inverse problems of geoelectrical exploration using the profiling method. Geodynamics. **1** (36), 98–107 (2024).

Розв'язування оберненої задачі теорії потенціалу каскадним алгоритмом та методом пригранічних елементів

Журавчак Л. М.[1], Забродська Н. В.[2]

[1] *Національний університет "Львівська політехніка", вул. С. Бандери, 12, 79013, Львів, Україна*
[2] *Карпатське відділення Інституту геофізики ім. С. І. Субботіна НАН України, вул. Наукова, 3б, Львів, 79060, Україна*

Обґрунтовано ефективність непрямого методу пригранічних елементів (як варіанту методу граничних інтегральних рівнянь) для побудови числових розв'язків прямої та оберненої задач теорії потенціалу в обмеженому кусково-однорідному об'єкті довільної форми, складові якого перебувають в ідеальному контакті. Інтегральне подання розв'язку прямої задачі побудовано з використанням фундаментального розв'язку рівняння Лапласа для площини. Для знаходження інтенсивностей невідомих джерел, уведених у пригранічних елементах, використано колокаційну методику, тобто крайові умови першого та другого роду та умови ідеального контакту задоволено у середині кожного граничного елемента. Після розв'язання отриманої системи лінійних алгебраїчних рівнянь знайдено шуканий потенціал у середовищі й включеннях та потік через їхні межі, враховуючи, що складові розглянуто як цілком незалежні області. За характером зміни потенціалу чи похідної від нього визначено початкові наближення для провідності включень, їхніх центрів мас, орієнтації та розмірів. Для розв'язання оберненої задачі побудовано алгоритм розпізнавання основних фізичних та геометричних характеристик включень за надлишковими даними потенціалу або потоку на межі об'єкта, який складається з двох каскадів ітерацій: у першому уточнено місцезнаходження локальних неоднорідностей та їхніх приблизних розмірів, у другому – їхню форму та орієнтацію на площині. Проведено обчислювальний експеримент для задачі електророзвідки постійним штучним полем методом опору, зокрема, електропрофілюванням.

Ключові слова: *математичне моделювання; теорія потенціалу; обернена задача; метод пригранічних елементів; кусково-однорідний об'єкт; електричне профілювання.*